EDGE ARTICLE

Check for updates

Molecular-level insight in supported olefin metathesis catalysts by combining surface organometallic chemistry, high throughput experimentation, and data analysis†

Jordan De Jesus Silva, [ID] [a] Marco A. B. Ferreira, [bc] Alexey Fedorov, [ID] *[ad] Matthew S. Sigman [ID] *[b] and Christophe Copéret [ID] *[a]

A combination of high-throughput experimentation (HTE), surface organometallic chemistry (SOMC) and statistical data analysis provided the platform to analyze *in situ* silica-grafted Mo imido alkylidene catalysts based on a library of 35 phenols. Overall, these tools allowed for the identification of σ-donor electronic effects and dispersive interactions and as key drivers in a prototypical metathesis reaction, homodimerization of 1-nonene. Univariate and multivariate correlation analysis confirmed the categorization of the catalytic data into two groups, depending on the presence of aryl groups in *ortho* position of the phenol ligand. The initial activity (TOF_{in}) was predominantly correlated to the σ-donor ability of the aryloxy ligands, while the overall catalytic performance ($TON_{1 h}$) was mainly dependent on attractive dispersive interactions with the used phenol ligands featuring aryl *ortho* substituents and, in sharp contrast, repulsive dispersive interactions with phenol free of aryl *ortho* substituents. This work outlines a fast and efficient workflow of gaining molecular-level insight into supported metathesis catalysts and highlights σ-donor ability and noncovalent interactions as crucial properties for designing active d^0 supported metathesis catalysts.

Introduction

Research in academic and industrial laboratories over the last several decades has produced impressive advances in the field of alkene metathesis.[1–6] This research has helped establishing detailed structure–activity relationships (SAR) for well-defined Mo-, W- and Ru-based molecular catalysts,[7,8] and thereby aided in the rational development of catalytic systems with improved activity, selectivity and stability.[9–11] Within this, high-throughput experimentation (HTE) can accelerate building robust SAR as it allows for a rapid and systematic acquisition of data on large libraries of compounds and formulations enabling the identification of catalysts.[12–17] Utilization of robotized HTE methods for data acquisition is particularly advantageous because they allow obtaining reproducible data

sets that are statistically significant to uncover robust and specific ligand properties in catalytic processes. We have recently integrated HTE with statistical analysis tools, inspired by methods of physical organic chemistry, that allow correlating various experimental and calculated steric or electronic ligand descriptors to performance indicators.[11,18] These reaction outputs include turnover numbers and frequencies (TONs and TOFs, respectively) as well as selectivity and stability.[8,10,18–25]

As an example of exploiting this methodology, we investigated the selective ethenolysis of cyclic olefins that relied on evaluating 29 well-defined Ru metathesis catalysts *via* HTE tools interfaced with statistical modeling. This effort ultimately provided a rational for the relative performance of catalysts, wherein the importance of π-backbonding and the size of the supporting NHC ligand for the selective formation of α,ω-dienes was revealed (Fig. 1).[7] We also recently reported, using a similar methodology, the importance of noncovalent interactions (NCI) in controlling the activity and the stability of Schrock-type metathesis catalysts.[8] Of particular note, the catalytic performance could be categorized by the type of phenols used to initiate the catalytic processes, wherein attractive non-covalent interactions (NCIs) were found to predominantly impact performance of catalysts that contained simple phenols devoid of *ortho*-aryl substituents. While powerful, this methodology has so far been rarely applied to the development and understanding of heterogeneous metathesis catalysts.[26,27]

[a]Department of Chemistry and Applied Biosciences, ETH Zürich, Vladimir-Prelog-Weg 1 5, CH 8093 Zürich, Switzerland. E-mail: ccoperet@ethz.ch; fedoroal@ethz.ch

[b]Department of Chemistry, University of Utah, 315 South 1400 East, Salt Lake City, Utah 84112, USA. E-mail: matt.sigman@utah.edu

[c]Centre for Excellence for Research in Sustainable Chemistry (CERSusChem), Department of Chemistry, Federal University of São Carlos – UFSCar, Rodovia Washington Luís, Km 235, SP-310, São Carlos, São Paulo, 13565-905, Brazil

[d]Department of Mechanical and Process Engineering, ETH Zürich, Leonhardstrasse 21, CH 8092 Zürich, Switzerland

† Electronic supplementary information (ESI) available. See DOI: 10.1039/d0sc02594a
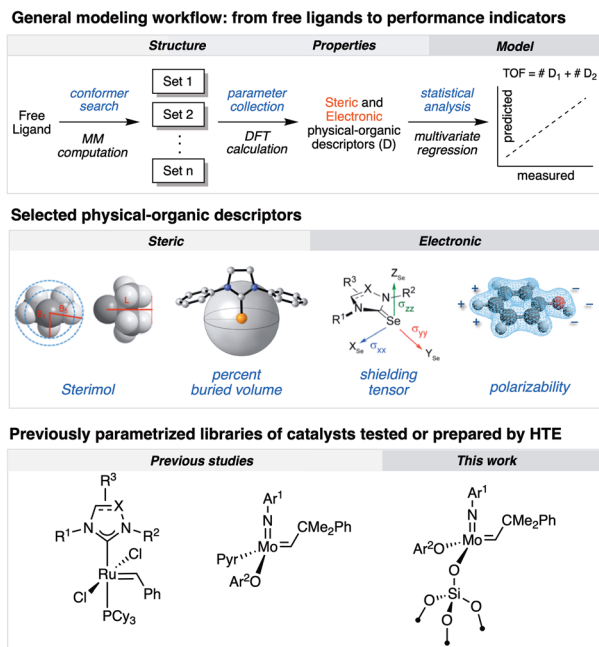
Fig. 1 The concept of integrating HTE with statistical modeling.

In parallel, surface organometallic chemistry (SOMC) has been established as a powerful approach to generate well-defined heterogeneous catalysts where the ligand effects can be probed.[9] In this approach, the surface is exploited as a ligand to anchor (covalently graft) molecular catalysts. One of the most prominent examples of SOMC is the development of silica-supported catalysts, wherein surface silanols are used to graft the molecular complex *via* protonolysis of an anionic ligand of the molecular precursor.[4,28] Besides the classical advantage of supported catalysts (ease of separation and recycling), this approach exploits surface site isolation to avoid bimolecular deactivation pathways, thereby increasing the stability of the corresponding well-defined supported catalysts compared to their homogenous analogues. In addition, these supported catalysts often feature activities exceeding those of their molecular counterparts.[29–34]

Herein, we demonstrate that combining HTE-SOMC[13] with data analysis aiming at the correlation of molecular properties is a powerful approach to understand the catalytic performance of silica-supported metathesis catalysts at the molecular level, using the homodimerization of 1-nonene as a prototypical reaction. Within this study, by applying multivariate statistical modeling, we reveal that NCIs, which are typically associated with molecular catalyst, also govern the catalytic activity of heterogeneous, silica-supported Schrock-type catalysts.

Results and discussion

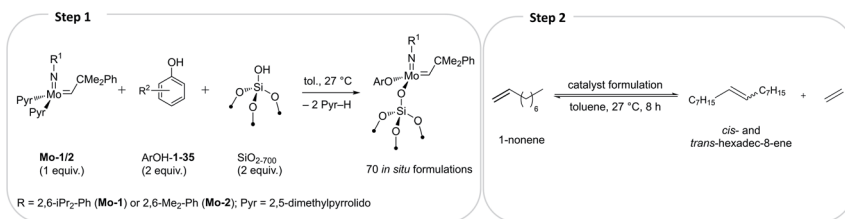### Testing *in situ* grafted Mo metathesis catalysts in the homodimerization of 1-nonene

To initiate this study, *in situ* formulations of a range of catalysts were prepared using 35 phenols with two precursor bis-pyrrolido Mo alkylidene complexes $(2,5\text{-}(Me)_2\text{-}Pyr)_2Mo(=$

$NAr)(=CHCMe_2Ph)$, where $Ar = 2,6\text{-}(i\text{-}Pr)_2\text{-}Ph$ (**Mo-1**) and $2,6\text{-}(Me)_2\text{-}Ph$ (**Mo-2**), and silica partially dehydroxylated at 700 °C $(SiO_{2\text{-}700})$ using HTE automation tools. The phenol library was designed on the basis of our previous studies.[8] The formulations were prepared using, 2 : 1 : 2 molar ratio of ArOH, **Mo-1/2** and $\equiv SiOH$ sites of $SiO_{2\text{-}700}$ support, respectively, in order to complete the ligand exchange and surface grafting, targeting *in situ* synthesis of monoaryloxide surface-grafted species (Fig. 2A and see also S2A†). Specifically, bis-pyrrolides **Mo-1** or **Mo-2** (1 equiv.) were contacted with each phenol (2 equiv.) in toluene for 5 minutes prior to adding the resultant solution to $SiO_{2\text{-}700}$ (2 equiv. of the surface $\equiv SiOH$), which was followed by keeping each reaction mixture for 3 h at 27 °C. We have recently shown using *in situ* ^1H NMR experiments that reacting **Mo-1** in a 1 : 2 ratio with various ArOH used in this work typically leads to the formation of a single new alkylidene resonance.[8] We reasoned that irrespective of the initial identity of the molecular alkylidene species present in solution (*i.e.* mono-aryloxide pyrrolide (MAP) or bisaryloxide species), the grafting reaction with $SiO_{2\text{-}700}$ will lead to the monografted aryloxy Mo species (Fig. 2A), owing to the known exclusive exchange of the pyrrolide ligand in preference to aryloxide ligand during grafting of MAP complexes.[35] In all cases, as the grafting reaction proceeds, the solution becomes colourless while the silica-supports becomes coloured. Prior to the catalytic test, all materials were washed to remove possible physisorbed molecular species on the silica material (see ESI† for details). Subsequently, a solution of 1-nonene in toluene was added to each *in situ* grafted material (0.1 mol% catalyst loading assuming quantitative grafting). All these steps were performed by an automated liquid handling robotic system operated inside an inert (N_2) atmosphere glovebox. The reaction mixtures were agitated at 27 °C in open vials while GC aliquots were automatically withdrawn for analysis after *ca.* 6, 16, 39, 72, 135, 258 and 501 minutes, giving conversion of 1-nonene (X), selectivity to hexadec-8-ene (S_{C16} and S_{C16} (E/Z)), and respective TONs and TOFs that are reported based on the yield hexadec-8-ene. Complete catalytic data is presented in the ESI (Tables S1, S2, Fig. S3–S5 and S12–S83).† Robustness tests were performed in triplicates with new batches of 1-nonene, exhibiting good reproducibility (Tables S3 and S4†). In the discussion below, we focus on two selected activity indicators, TOF_{in} and $TON_{1\ h}$ (data points collected after *ca.* 6 and 72 min, respectively). TOF_{in} reflects the initial activity of the catalyst formulation. Given that formulations on average reach $X_{1\ h} > 40\%$ after 72 min but no formulation reaches full conversion at this time point, the $TON_{1\ h}$ indicator provides information about catalyst stability (Fig. 2, see ESI† for such plots using results with **Mo-2**).

Control experiments performed using longer premixing of various selected phenols and **Mo-1** prior to contacting with $SiO_{2\text{-}700}$ (*i.e.* 180 *vs.* 5 min, 2 : 1 : 2 molar ratio, respectively, Table S5†) show no notable differences in catalytic results beyond experimental error, which suggest formation of the same grafted species irrespective of premixing time. This indicates that even if the starting unreacted bis-pyrrolide complex **Mo-1** might graft onto $SiO_{2\text{-}700}$ faster than the pyrrolide ligand exchanges with ArOH, the latter ligand exchange can also proceed on the

A. *In-situ*-generated molybdenum alkylidene complexes for homodimerization of 1-nonene (steps 1-2)

C. Results for the catalytic homodimerization of 1-nonene with formulation prepared from Mo-1, ArOH 1–35 and SiO$_{2\text{-}700}$ (1:2:2 ratio, see ESI for details)

B. Library of phenol ligands

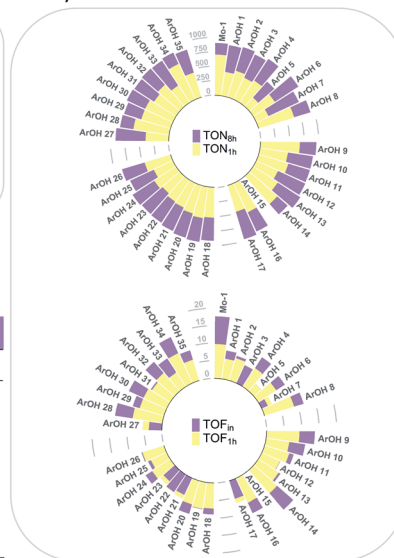| Group A (no aryl arms)				Group B (with aryl arms)			
R^2-Ph in Ar–OH	Code	R^2-Ph in Ar–OH	Code	R^2-Ph in Ar–OH	Code	R^2-Ph in Ar–OH	Code
2-F	**1**	2,6-iPr	**11**				
2,6-Me	**2**	2,3,4,5,6-F	**12**	2,6-Ph	**21**	2,6-Mes-4-F	**29**
2-F-6-Me	**3**	2,4,6-Cl	**13**	2,6-Ph-4-Me	**22**	2,3,5,6-Ph	**30**
4-Cl	**4**	2,6-tBu	**14**	2,6-Ph-4-F	**23**	3,3'-Br-2'-MeO-napht	**31**
3,5-F	**5**	2,6-NO$_2$-4-CF$_3$	**15**	2-Br-6-Mes	**24**	2,3,5,6-Ph-4-Br	**32**
2,4,6-F	**6**	2,6-Br-4-Me	**16**	2,6-(2-MeO-Ph)	**25**	2,6-(3,5-CF$_3$-Ph)	**33**
2,6-MeO	**7**	2,3,4,5,6-Cl	**17**	2,4,6-Ph	**26**	2,6-(2,5-Ph-Pyr)	**34**
2-CF$_3$	**8**	2,6-Br-4-F	**18**	2,6-Ph-4-Br	**27**	3,3'-Br-2-TBDMS-napht	**35**
4-CF$_3$	**9**	2,4,6-Br	**19**	2,6-Mes	**28**		
4-Br	**10**	2,3,4,5,6-Br	**20**				

Fig. 2 Design of the HTE study (A and B) and catalytic results (C) for *in situ* grafted formulations with Mo-1 with ArOH 1–35.

grafted **Mo-1**/SiO$_{2\text{-}700}$ species. To confirm this, we have contacted well-characterized **Mo-1**/SiO$_{2\text{-}700}$ material described previously[15] with 2 equiv. of ArOH-**2** or **13** and followed the reaction by *in situ* ^{1}H NMR spectroscopy. Quantifications of released 2,5-dimethylpyrrole in solution shows that with ArOH-**2** or **13**, the exchange proceeds quantitatively within 3 hours. However, the exchange reaction is accompanied by a partial de-grafting (7 and 14% for ArOH-**2** or **13**, respectively, Table S6†) as indicated by the alkylidene signal of bisaryloxide alkylidene species in solution. Thus, we conclude that the exchange of the 2,5-dimethylpyrrolide ligand for the aryloxide ligand also proceeds in the grafted **Mo-1**/SiO$_{2\text{-}700}$ species, which leads to the target grafted aryloxide species in these *in situ* prepared formulations. Because the washing step implemented in the *in situ* grafting protocol removes soluble molecular alkylidene species, the measured catalytic activity discussed below is predominantly due to the grafted aryloxide surface species (Fig. 2A).

Comparison between formulations with **Mo-1** and **Mo-2** for TOF$_{in}$ or TON$_{1\text{ h}}$ reveals that *in situ* catalysts derived from the smaller 2,6-dimethylphenylimido ligand (**Mo-2**) exhibit significantly reduced TOF$_{in}$ and TON$_{1\text{ h}}$ (Fig. 2, S4 and S5†). This trend is consistent with our previous results on inferior activity of homogeneous formulations derived from **Mo-2** in the self-metathesis of 1-nonene.[8] Here, we observe that phenols without aryl groups in *ortho* positions (Fig. 2B, Group A) in general lead to lower activities (Fig. S4†). However, phenols with pendant aryls (Group B) yield similarly activities irrespective of the size of the imido moiety. In what follows, for brevity we concentrate the discussion on the results obtained with **Mo-1**.

In situ grafting of **Mo-1** onto SiO$_{2\text{-}700}$ leads to a formulation (**Mo-1**/SiO$_{2\text{-}700}$, mono-siloxide pyrrolide species) featuring TOF$_{in}$ = 17.7 min^{-1} and TON$_{1\text{ h}}$ = 700, which is notable as unsupported **Mo-1** is nearly inactive. Grafting of **Mo-1** in the presence of phenols **1–35** gives formulations with TOF$_{in}$ and TON$_{1\text{ h}}$ values generally lower than those of **Mo-1**/SiO$_{2\text{-}700}$ or respective molecular formulations. However, almost every grafted formulation reaches conversions exceeding 95% after 8 h with an average S_{C16} selectivity for all 35 ligands at 97% and 94% after 1 h and 8 h, respectively. Comparison of $E/Z_{8\text{ h}}$, TOF$_{in}$, TON$_{1\text{ h}}$, and TON$_{8\text{ h}}$ between *in situ* prepared silica-supported and respective molecular formulations reveal that while the initial rate of the *in situ* grafted formulations is reduced relative to molecular formulations, the deactivation is generally retarded for grafted catalysts, as assessed by the narrow range of TON$_{1\text{ h}}$ around approximately 480 (Fig. S9†). This is presumably due to the suppression of bimolecular deactivation pathways for site-isolated grafted metathesis catalysts.[31–34]

TOF$_{in}$ and TON$_{1\text{ h}}$ values for formulations based on **Mo-1** are correlated with $R^2 = 0.73$, which suggests similar deactivation pathways/relative rates for most ligands (Fig. S7†). For all formulations, the (E/Z) ratios for the S_{C16} (E) isomer increase as the reaction progresses, approaching the thermodynamic ratio S_{C16} $(E/Z)_{8\text{ h}} = 5.25$ (84 : 16 *trans* : *cis* product). No highly *Z*-selective catalyst formulations were formed using SiO$_{2\text{-}700}$ as a support, in contrast to what was observed previously with molecular systems where ArOH-**28**, **33**, **34** and **35** gave *Z*-selective formulations (Fig. S9†).[8,36–40] The highest *Z*-selectivity of *ca.* 40% was found for the grafted formulation derived from **Mo-1** and ArOH-**5**; this selectivity, however, was stable during the catalytic test.

Univariate modeling

In order to compare differences between the trends reported for homogeneous systems derived from **Mo-1** and the grafted

aryloxides, we used the same set of molecular descriptors of the phenolic ligands as in our previous study.[8] We started by classifying the $TON_{1\,h}$ catalytic data according to the nature of substituents on the phenol ligands to those without and with aryl groups in *ortho* positions of ArOH (Groups A and B in Fig. 2, respectively). This was accomplished using the Sterimol parameter L_{sum}, which quantifies steric volume along the axes of both *ortho* substitutes in aryloxide ligands.[41] Parameter L_{sum} indicates different catalytic regimes for the respective subsets of ligands in the grafted formulations and is in line with our previous findings on respective molecular analogues (Fig. S8†).[8]

Analysis of outliers and control experiments

Analysis of the univariate correlations also uncovered systematic outliers that were excluded for further analysis. As in our previous study, (2,6-NO_2-4-CF_3)-PhOH **15** yielded an inactive formulation, likely owing to protonation of the alkylidene.[8] Phenols with an increasingly large size such as ArOH-**14**, ArOH-**28** or ArOH-**34**, were identified as slow exchangers in our previous study,[8] and provided materials with TOF_{in} similar to that of the control catalyst, **Mo-1**/SiO_{2-700}. This suggests that the exchange has likely proceeded only to a low extent, resulting in the same grafted species in **Mo-1**/SiO_{2-700} and with formulations containing phenols ArOH-**14, 28, 34** (Fig. 2C and Table S1†).

Formulations with low TOF are observed for phenols with *ortho*-methoxy substituents (ArOH-**7** and **25**), likely due to coordination of this group to Mo and blocking the olefin coordination site.[8] With that said, $TON_{8\,h}$ values reached by these formulations are similar to formulations with other tested phenols. This can be explained by the generally improved stability of grafted catalysts. Interestingly, three particular outliers were identified (Fig. S8†), involving the fluorine-bearing ligands 3,5-F-PhOH, 2-CF_3-PhOH and 4-CF_3-PhOH (ArOH-**5, 8** and **9**, respectively). Formulations with ArOH-**5** show lower activity than other Group A ligands, whereas ArOH-**8** and ArOH-**9** display high activity, reminiscent of grafted **Mo-1** without addition of an ArOH ligand. We speculate that fluorine interactions with the silica surface are at the origin of these observations. In particular, the exchange of the aryloxide ligand between **Mo-1**/SiO_{2-700} and ArOH-**9** is hindered, proceeding to only 18% after 3 h according to *in situ* ^1H NMR experiment (Table S6†), and in contrast to what was observed for ArOH-**2** or **13** discussed above. However, while a quantitative exchange is observed between **Mo-1**/SiO_{2-700} and ArOH-**5**, low activity of this formulation is likely due to the fluorine–silica interaction. As described above, ArOH-**5** provides the most *Z*-selective catalyst among all tested formulations.

Correlations of *ortho*-isosteric ligands

To further examine the robustness of the acquired experimental data and the electronic impact of aryloxides, univariate intercorrelations within the data set were analyzed. Therefore, subclasses of phenols bearing the same *ortho* substituents were selected following insight from our earlier work:[8] phenols with the 2,6-dibromo and 2,6-diphenyl ligands (ArOH-**16, 18, 19, 20** from Group A, and ArOH-**21, 22, 23, 26, 27, 30, 32** from Group
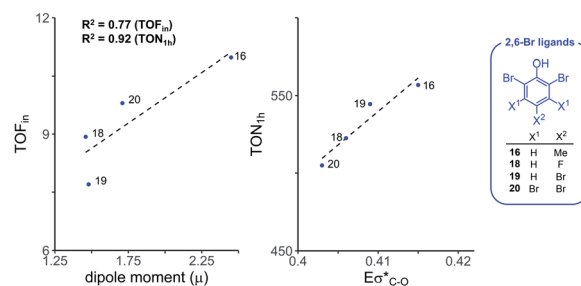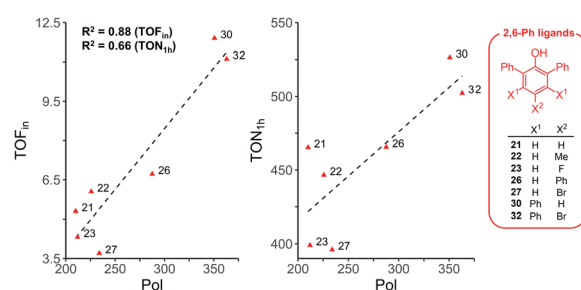

Fig. 3 Univariate correlation of electronic descriptors for selected formulations using **Mo-1** and ligands without (A) and with (B) *ortho* aryl substituents.

B). Analysis of 2,6-Br ligands (Fig. 3A) identifies a good correlation of TOF_{in} and the dipole moment μ, with a commensurate increase in TOF_{in} as the permanent charge separation within the ligand is enhanced. This is possibly related to σ-donor abilities of the ligand. In contrast, an excellent correlation is observed between $TON_{1\,h}$ and the antibonding $\sigma^*_{(C-O)}$ NBO energies ($E\sigma^*_{(C-O)}$, $R^2 = 0.92$, Fig. 3A), marked by an increase in turnover number with increasing electron density on the pendant aryl substituents. This reflects the σ-donation due to inductive effects of the substituents on the phenol ring. Analogous analysis of the 2,6-Ph series of phenols reveals that increasing the polarizability enhances the rates and turnover numbers, as defined by a correlation between TOF_{in} and $TON_{1\,h}$ with Pol parameter ($R^2 = 0.88$ and 0.66, respectively, Fig. 3B).

Overall, this data suggests that electronic effects (as reflected in μ and $E\sigma^*_{(C-O)}$ parameters) are key factors for Group A ligands. Group B on the other hand, is impacted by the polarizability Pol, a descriptor with hybrid character expected for ligands of larger size, for which attractive interactions with the silica surface could potentially be important.[42]

Multivariate regression analysis

The assessment of cooperative effects on the catalytic performance was investigated though multivariate linear regression analysis on the TOF_{in} and $TON_{1\,h}$ responses for Group A and B (Fig. 4, Table S7 and 8†). The consistency of the models is probed with internal-validation techniques (leave-one-out (LOO) and *k*-fold methods), yielding good scores for all cases consistent with a well-validated model.[7–9] The trained models from normalized descriptors gave coefficients that revealed the significance of each of represented effects.
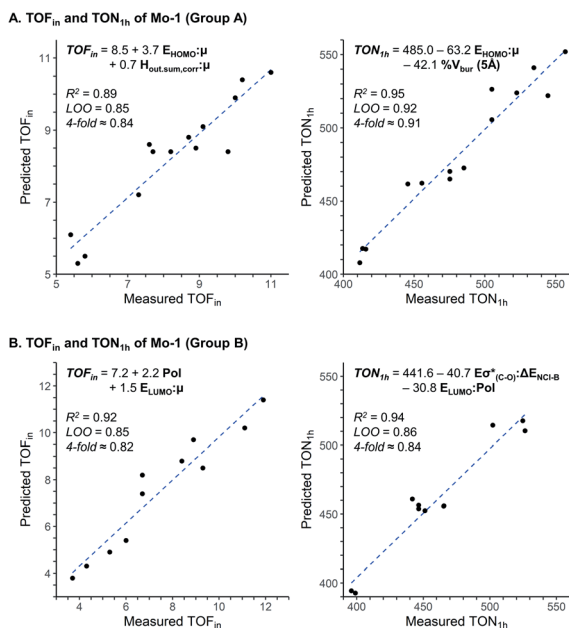
A. TOF_{in} and TON_{1h} of Mo-1 (Group A)

$TOF_{in} = 8.5 + 3.7\ E_{HOMO}:\mu$
$+ 0.7\ H_{out.sum.corr}:\mu$

$R^2 = 0.89$
$LOO = 0.85$
$4\text{-}fold \approx 0.84$

$TON_{th} = 485.0 - 63.2\ E_{HOMO}:\mu$
$- 42.1\ \%V_{bur}\ (5\text{Å})$

$R^2 = 0.95$
$LOO = 0.92$
$4\text{-}fold \approx 0.91$

B. TOF_{in} and TON_{1h} of Mo-1 (Group B)

$TOF_{in} = 7.2 + 2.2\ Pol$
$+ 1.5\ E_{LUMO}:\mu$

$R^2 = 0.92$
$LOO = 0.85$
$4\text{-}fold \approx 0.82$

$TON_{th} = 441.6 - 40.7\ E\sigma^*_{(C\text{-}O)}:\Delta E_{NCI\text{-}B}$
$- 30.8\ E_{LUMO}:Pol$

$R^2 = 0.94$
$LOO = 0.86$
$4\text{-}fold \approx 0.84$

Fig. 4 Multivariate linear regression model to predict TOF_{in} and $TON_{1\ h}$ for Group A (A) and Group B (B).

The multivariate models obtained for the Group A feature steric and electronic hybrid interactions terms for TOF_{in} and $TON_{1\ h}$ (Fig. 4A and B). Consistent with our previous results on molecular catalysts,[8] the electronic effect is dominant for both TOF_{in} and $TON_{1\ h}$. The first descriptor, that includes μ and $HOMO_{phenol}$, has the highest significance in both models. This interaction term describes the σ-donor ability of the aryloxy ligand; it is expected that stronger σ-donor ligands (less negative interaction term) increase the activity of the complex by increasing the electronic dissymmetry at the metal centre and their higher *trans*-influence with respect to the weaker σ-donating surface siloxy ligand.[43–45] The hybrid stereoelectronic descriptor used for modeling TOF_{in}, an interaction term of μ and $H_{out,sum,corr}$, reflects the perturbation of the permanent dipole by the electron density of the pendant substituents on the phenolic ligands. This steric descriptor captures the increase in catalytic activity by the repulsive NCI exerted by *ortho* pendant substituents. Notably, the steric effects gain in importance with increasing reaction times as indicated by the inclusion of % V_{bur} (5 Å) in the $TON_{1\ h}$ model.

Consequently, statistical modeling was also employed for Group B. The correlations found for the TOF_{in} and $TON_{1\ h}$ responses showcase a strong significance of the polarizability Pol of the ligands, as indicated by the large coefficient (Fig. 4B). The polarizability could possibly be an effect of the silica surface (attractive interaction of the surface with aryl moiety).[46] In the model for TOF_{in}, the polarizability appears as a single term, accompanied by an interaction term ($LUMO_{phenol}$ and μ), that can be viewed again as the σ-donor ability of the phenol oxygen. This is in line with the previous empirical observation that stronger σ-donors produced higher catalytic activity, as illustrated by the electron-rich 2,6-Ph ligands of Group B (Fig. 3).

Evaluation of the $TON_{1\ h}$ response shows that the polarizability appears in an interaction term (Pol and $LUMO_{phenol}$), together with a second stereoelectronic descriptor ($E\sigma^*_{(C–O)}$ and $\Delta E_{NCI\text{-}B}$). The LUMO and $E\sigma^*_{(C–O)}$ essentially describe related phenomena due to the perturbation of the electron density by pendant substituents with varying electronic properties. The non-covalent interaction term $\Delta E_{NCI\text{-}B}$ not only modulates the decrease of activity with the increase of size of ligand, but in concert with the polarizability, highlights the importance of dispersive forces in enhancing catalytic performance.

Conclusions

In summary, we developed a practical protocol based on high-throughput experimentation combined with surface organo-metallic chemistry that allows generating and testing the catalytic performance of large libraries of *in situ* grafted Mo imido alkylidene metathesis catalyst, based on 35 phenol ligands and two precursor Mo bis-pyrrolido alkylidene complexes. Control experiments indicated that grafted aryloxide Mo alkylidene surface species were formed. Using statistical data analysis, we identified σ-donation ability of the ligands and dispersive forces to be essential in promoting catalytic activity. Univariate modeling allowed distinguishing two groups of phenoxy ligands, either without aryl arms in *ortho* position (Group A) or with aryl arms in ortho position (Group B). This finding on supported catalysts is reminiscent of what is observed in the corresponding libraries of molecular catalysts, indicating that catalysts prepared by SOMC retained a molecular character. In comparison to their molecular counterparts, all grafted catalysts display lower initial rates (as evaluated by TOF_{in}), but higher stability as seen by a narrow range of $TON_{1\ h}$ approximately 480. After 8 h of reaction, 44 from 70 grafted catalyst formulations reached conversion of 1-nonene exceeding 90% (as opposed to only 31 formulations for molecular *in situ* prepared formulations). This is likely due to higher stability of grafted species, as site-isolated metathesis catalysts do not suffer from bimolecular deactivation pathways.[47] Overall the initial rates for both groups are dominated by the σ-donor ability of the aryloxy ligands, supporting the view that electronic dissymmetry at the metal centre improves the activity of Schrock-type metathesis catalysts by facilitating coordination of the olefin substrate as well as the retrocyclization. However, as reaction times increase, opposite trends in the catalytic performance (as evaluated by $TON_{1\ h}$) arise with an increase of the *ortho* pendant substituent size. While for Group A the increase in steric bulk (described by % V_{bur} (5 Å)) is associated with lower turnover numbers, Group B displays an increase in catalytic performance with increasing steric bulk, likely owing to non-covalent interactions of the aryl moieties with the silica surface. This work showcases how molecular aspects of heterogeneous catalysts prepared *via* an HTE-SOMC approach can be evaluated *via* statistical methods. We confirmed that grafting enhances the stability of metathesis catalysts and corroborated that promoting electronic dissymmetry at the metal centre by modulating the σ-donor ability of the aryloxy ligands increases activity. Furthermore, we highlighted the

importance of dispersive interaction of ligands, aryl alcohols or silica support, in enhancing the catalyst activity in grafted d^0 metathesis catalysts.

Conflicts of interest

There are no conflicts to declare.

Acknowledgements

Notes and references

1 R. H. Grubbs, *Handbook of Metathesis*, Wiley-VCH, Weinheim, 2014.

2 C. S. Higman, J. A. M. Lummiss and D. E. Fogg, *Angew. Chem., Int. Ed.*, 2016, **55**, 3552.

3 E. S. Sattely, S. J. Meek, S. J. Malcolmson, R. R. Schrock and A. H. Hoveyda, *J. Am. Chem. Soc.*, 2009, **131**, 943–953.

4 C. Copéret, F. Allouche, K. W. Chan, M. P. D. Conley, F. Murielle, A. Fedorov, I. B. Moroz, V. Mougel, M. Pucino, K. Searles, K. Yamamoto and P. A. Zhizhko, *Angew. Chem., Int. Ed.*, 2018, **57**, 6398.

5 A. H. Hoveyda, *J. Org. Chem.*, 2014, **79**, 4763.

6 M. J. Benedikter, F. Ziegler, J. Groos, P. M. Hauser, R. Schowner and M. R. Buchmeiser, *Coord. Chem. Rev.*, 2020, **415**, 213315.

7 P. S. Engl, C. B. Santiago, C. P. Gordon, W. C. Liao, A. Fedorov, C. Copéret, M. S. Sigman and A. Togni, *J. Am. Chem. Soc.*, 2017, **139**, 13117.

8 M. A. B. Ferreira, J. De Jesus Silva, S. Grosslight, A. Fedorov, M. S. Sigman and C. Copéret, *J. Am. Chem. Soc.*, 2019, **141**, 10788–10800.

9 V. Mougel, C. B. Santiago, P. A. Zhizhko, E. N. Bess, J. Varga, G. Frater, M. S. Sigman and C. Copéret, *J. Am. Chem. Soc.*, 2015, **137**, 6699.

10 J. Y. Guo, Y. Minko, C. B. Santiago and M. S. Sigman, *ACS Catal.*, 2017, **7**, 4144.

11 C. B. Santiago, J. Y. Guo and M. S. Sigman, *Chem. Sci.*, 2018, **9**, 2398.

12 S. T. Alvaro Gordillo, C. Futter, M. L. Lejkowski, E. Prasetyo, T. Luis, A. Rupflin, T. Emmert and S. A. Schunk, *High-Throughput Experimentation in Catalysis and Materials Science*, Wiley-VCH, Weinheim, 2014.

13 R. Arancon, M. Saab, A. Morvan, A. Bonduelle-Skrypczak, A.-L. Taleb, A.-S. Gay, C. Legens, O. Ersen, K. Searles, V. Mougel, A. Fedorov, C. Copéret and P. Raybaud, *J. Phys. Chem. C*, 2019, **123**, 24659–24669.

14 A. Fedorov, H.-J. Liu, H.-K. Lo and C. Copéret, *J. Am. Chem. Soc.*, 2016, **138**, 16502–16507.

15 P. A. Zhizhko, V. Mougel, J. De Jesus Silva and C. Copéret, *Helv. Chim. Acta*, 2018, **101**, e1700302.

16 S. Monfette, J. M. Blacquiere and D. E. Fogg, *Organometallics*, 2011, **30**, 36–42.

17 P. Wyrębek, P. Małecki, A. Sytniczuk, W. Kośnik, A. Gawin, J. Kostrzewa, A. Kajetanowicz and K. Grela, *ACS Omega*, 2018, **3**, 18481–18488.

18 F. D. Toste, M. S. Sigman and S. J. Miller, *Acc. Chem. Res.*, 2017, **50**, 609.

19 C. B. Santiago, A. Milo and M. S. Sigman, *J. Am. Chem. Soc.*, 2016, **138**, 13424.

20 C. A. Hollingsworth, P. G. Seybold and C. M. Hadad, *Int. J. Quantum Chem.*, 2002, **90**, 1396.

21 A. Verloop and E. J. Ariens, *Drug Design*, 1976.

22 A. C. Hillier, W. J. Sommer, B. S. Yong, J. L. Petersen, L. Cavallo and S. P. Nolan, *Organometallics*, 2003, **22**, 4322.

23 M. Orlandi, J. A. S. Coelho, M. J. Hilton, F. D. Toste and M. S. Sigman, *J. Am. Chem. Soc.*, 2017, **139**, 6803.

24 A. J. Neel, M. J. Hilton, M. S. Sigman and F. D. Toste, *Nature*, 2017, **543**, 637.

25 J. P. Wagner and P. R. Schreiner, *Angew. Chem., Int. Ed.*, 2015, **54**, 12274.

26 M. Stoyanova, U. Rodemerck, U. Bentrup, U. Dingerdissen, D. Linke, R. W. Mayer, H. G. J. Lansink Rotgerink and T. Tacke, *Appl. Catal., A*, 2008, **340**, 242–249.

27 D. R. Romer, V. J. Sussman, K. Burdett, Y. Chen and K. J. Miller, *ACS Comb. Sci.*, 2014, **16**, 551–557.

28 C. Copéret, A. Comas-Vives, M. P. Conley, D. P. Estes, A. Fedorov, V. Mougel, H. Nagae, F. Núñez-Zarur and P. A. Zhizhko, *Chem. Rev.*, 2016, **116**, 323–421.

29 N. Rendón, F. Blanc and C. Copéret, *Coord. Chem. Rev.*, 2009, **253**, 2015–2020.

30 C. Copéret, *Dalton Trans.*, 2007, 5498–5504.

31 J. Robbins, G. C. Bazan, J. S. Murdzek, M. B. O'Regan and R. R. Schrock, *Organometallics*, 1991, **10**, 2902–2907.

32 L. P. H. Lopez and R. R. Schrock, *J. Am. Chem. Soc.*, 2004, **126**, 9526–9527.

33 A. Sinha, L. P. H. Lopez, R. R. Schrock, A. S. Hock and P. Müller, *Organometallics*, 2006, **25**, 1412–1423.

34 L. P. H. Lopez, R. R. Schrock and P. Müller, *Organometallics*, 2006, **25**, 1978–1986.

35 N. Rendón, R. Berthoud, F. Blanc, D. Gajan, T. Maishal, J.-M. Basset, C. Copéret, A. Lesage, L. Emsley, S. C. Marinescu, R. Singh and R. R. Schrock, *Chem.–Eur. J.*, 2009, **15**, 5083–5089.

36 M. J. Koh, T. T. Nguyen, J. K. Lam, S. Torker, J. Hyvl, R. R. Schrock and A. H. Hoveyda, *Nature*, 2017, **542**, 80.

37 S. J. Meek, R. V. O'Brien, J. Llaveria, R. R. Schrock and A. H. Hoveyda, *Nature*, 2011, **471**, 461–466.

38 M. M. Flook, L. C. H. Gerber, G. T. Debelouchina and R. R. Schrock, *Macromolecules*, 2010, **43**, 7515–7522.

39 A. J. Jiang, Y. Zhao, R. R. Schrock and A. H. Hoveyda, *J. Am. Chem. Soc.*, 2009, **131**, 16630.

40 M. M. Flook, A. J. Jiang, R. R. Schrock, P. Müller and A. H. Hoveyda, *J. Am. Chem. Soc.*, 2009, **131**, 7962–7963.

41 A. V. Brethomé, S. P. Fletcher and R. S. Paton, *ACS Catal.*, 2019, **9**, 2313–2323.

42 F. Blanc, J.-M. Basset, C. Copéret, A. Sinha, Z. J. Tonzetich, R. R. Schrock, X. Solans-Monfort, E. Clot, O. Eisenstein, A. Lesage and L. Emsley, *J. Am. Chem. Soc.*, 2008, **130**, 5886–5900.

43 V. Mougel and C. Copéret, *Chem. Sci.*, 2014, **5**, 2475.

44 A. Poater, X. Solans-Monfort, E. Clot, C. Copéret and O. Eisenstein, *J. Am. Chem. Soc.*, 2007, **129**, 8207–8216.

45 X. Solans-Monfort, C. Copéret and O. Eisenstein, *Organometallics*, 2012, **31**, 6812.

46 B. Rhers, A. Salameh, A. Baudouin, E. A. Quadrelli, M. Taoufik, C. Copéret, F. Lefebvre, J.-M. Basset, X. Solans-Monfort, O. Eisenstein, W. W. Lukens, L. P. H. Lopez, A. Sinha and R. R. Schrock, *Organometallics*, 2006, **25**, 3554–3557.

47 F. Blanc, C. Copéret, J. Thivolle-Cazat, J.-M. Basset, A. Lesage, L. Emsley, A. Sinha and R. R. Schrock, *Angew. Chem., Int. Ed.*, 2006, **45**, 1216–1220.